# Fast pyrolysis with fractional condensation of lignin-rich digested stillage from second-generation bioethanol production

Priharto, Neil; Ronsse, Frederik; Yildiz, Güray; Heeres, Hero Jan; Deuss, Peter J.; Prins, Wolter

*Published in:*
Journal of Analytical and Applied Pyrolysis

*DOI:*
10.1016/j.jaap.2019.104756



*Publication date:*
2020

Journal of Analytical and Applied Pyrolysis 145 (2020) 104756

Contents lists available at ScienceDirect

Journal of Analytical and Applied Pyrolysis

journal homepage: www.elsevier.com/locate/jaap

# Fast pyrolysis with fractional condensation of lignin-rich digested stillage from second-generation bioethanol production

Neil Priharto[a,b], Frederik Ronsse[b], Güray Yildiz[c], Hero Jan Heeres[d], Peter J. Deuss[d], Wolter Prins[b,*]

[a] School of Life Sciences and Technology, Institut Teknologi Bandung, Jalan Ganesha 10, Bandung 40132, Indonesia
[b] Department of Green Chemistry & Technology, Ghent University, Coupure links 653, 9000 Gent, Belgium
[c] Department of Energy Systems Engineering, Izmir Institute of Technology, 35430 Urla-Izmir, Turkey
[d] Department of Chemical Engineering, University of Groningen, Nijenborgh 4, 9747 AG Groningen, the Netherlands

ARTICLE INFO

*Keywords:*
Lignin-rich digested stillage
Fast pyrolysis
Fractional condensation
Mechanically stirred bed
Pyrolysis liquids

ABSTRACT

Poplar-derived lignin-rich feedstock (i.e. stillage) obtained from bioethanol production was subjected to fast pyrolysis in a modified fluidised bed reactor at 430 °C, 480 °C, and 530 °C. The stillage was pretreated by enzymatic digestion prior to fast pyrolysis. Pyrolysis vapors were collected by fractional condensation to separate the heavy organic and aqueous phase liquids. The intention of this study was to assess the potential utilization of lignin-rich digested stillage as a fast pyrolysis feedstock. Heavy organic and aqueous phase pyrolysis liquids were obtained in yields ranging from 15.1–18.1 wt.% and 9.7–13.4 wt.% respectively. The rest of the feedstock material was converted to char (37.1–44.7 wt.%) and non-condensable gases (27.1–31.5 wt.%). Detailed liquid analysis indicated that the heavy organic phase fractions contain compounds arising from the degradation of lignin, residual microbial biomass and remaining polysaccharides. Fast pyrolysis adds 26.8 wt.% to the conversion of this otherwise recalcitrant feedstock material, thereby reducing waste generation and enhancing the value of second-generation bioethanol production.

## 1. Introduction

The Horizon 2020 Renewable Energy Directive of the European Commission mandated the EU Member States to achieve a 10 % renewable energy share in the transport sector by 2020, which is changing the renewables market and regulations. Directives lean more towards bioethanol production from second-generation (e.g. lignocellulosic) feedstock due to multiple benefits compared to those of first-generation feedstock. Besides the non-competitive nature of the feedstock with food production, second-generation bioethanol production also offers reduced greenhouse gas emissions, lower negative impact on soil and water quality, and it is theoretically carbon neutral [1–3]

Recent technology developments in the pretreatment of lignocellulosic biomass have managed to obtain almost 95 % conversion of cellulose and hemicellulose to sugars that can be further converted to bioethanol through saccharification and fermentation processes. Unfortunately, the lignin component of the biomass feedstock remains still mostly unused, thereby lowering the overall valorisation potential of the process. Some of the most commonly used lignocellulosic biomass feedstock types in second-generation bioethanol plants in Europe are poplar (*Populus sp.*) and hybrid poplar. According to previous studies, poplar contains around 22–27 % wt.% (d.b.) of lignin [4,5]. Common acid pre-treatment methods in bioethanol production are not able to efficiently depolymerise or physically remove the lignin contained in poplar, by which the bio-availability of the hemicellulose and cellulose fraction for further saccharification is limited. Kundu et al. [6] reported that even an “advanced” acid pretreatment of poplar could not reduce the lignin content or disrupt the lignin structures significantly.

This feedstock limitation coupled with the inefficiency of the pretreatment process results in the build-up of unprocessed solid stillage. This type of stillage is not only rich in lignin but also contains residual cellulose and hemicellulose portions. Further steps to utilise the poplar-derived lignin-rich stillage are either to use it as a solid fuel for Combined Heat and Power (CHP) generation or to feed it into a biogas digester. Anaerobic digestion for the production of biogas out of this stillage is attractive because of the successive valorisation of any residual cellulose or hemicellulose in the lignin-rich stillage. Lignin has been demonstrated to have low digestibility and low biogas potential

* Corresponding author,
*E-mail address:* Wolter.Prins@UGent.be (W. Prins).

https://doi.org/10.1016/j.jaap.2019.104756
Received 12 July 2019; Received in revised form 27 November 2019; Accepted 13 December 2019
Available online 14 December 2019
0165-2370/ 

**Nomenclature**

| | |
|---|---|
| $A_c$ | ash mass fraction in the char (wt.%) |
| $\Delta m_{loi}$ | weight difference of sand and char mixture before and after loss-on ignition (g) |
| $m_{a,h}$ | mass of aqueous phase in ESP collected pyrolysis liquid (g) |
| $m_{bm}$ | feedstock mass (g) |
| $m_{c,h}$ | mass of char in heavy phase pyrolysis liquid (g) |
| $m_{c,k}$ | mass of char in collected in knockout vessel (g) |
| $m_{con,i}$, $m_{con,f}$ | condenser flasks mass (g) before and after the pyrolysis experiment, respectively |
| $m_{c,rm}$ | mass of char that was removed for subsequent analysis (g) |
| $m_{ESP,i}$, $m_{ESP,f}$ | ESP mass (g) before and after the pyrolysis experiment, respectively |
| $m_{f,i}$ | $m_{f,f}$ cotton filter mass (g) before and after the pyrolysis experiment, respectively |
| $m_{h,a}$ | mass of heavy phase in condenser flask collected pyrolysis liquid (g) |
| $M_w$ | weight-average molecular weight (g $mol^{-1}$) |
| $M_n$ | number-average molecular weight (g $mol^{-1}$) |
| $\bar{Q}_b$ | average sweep gas volumetric flow rate (L $h^{-1}$) |
| $\bar{Q}_s$ | average volumetric gas flow during pyrolysis (L $h^{-1}$) |
| $\rho_{NCG}$ | density of non-condensable gases at outlet temperature (g $L^{-1}$) |
| $t$ | experiment time (h) |
| $w_C$ | mass fraction of carbon (wt.%) |
| $w_H$ | mass fraction of hydrogen (wt.%) |
| $w_N$ | mass fraction of nitrogen (wt.%) |
| $w_O$ | mass fraction of oxygen (wt.%) |
| $w_S$ | mass fraction of sulfur (wt.%) |
| $Y_{aqueous}$ | aqueous phase pyrolysis liquid yield (wt.% on dry feedstock basis) |
| $Y_{char}$ | char yield (wt. % on dry feedstock basis) |
| $Y_{NCG}$ | NCG yield (wt.% on dry feedstock basis) |
| $Y_{organic}$ | heavy phase pyrolysis liquid yield (wt.% on dry feedstock basis) |
| $Y_{tot}$ | total yield (wt.% on dry feedstock basis) |

compared to carbohydrates and carbohydrate-based polymers found in plant cell walls. The effectiveness of anaerobic digestion of lignin polymers depends on the feedstock's physicochemical properties as the structure of lignin allows only for limited access by micro-organisms or enzymes [7]. Multiple studies indicate that syringyl/guaiacyl ratios (S/G ratios) in lignin, molecular weight and the prevalence of β-O-4 linkage content determine the degradability of lignin in anaerobic digestion [7–9]. Barakat et al. [7] reported that only 2–7 % of lignin was converted to methane, while Benner et al. [9] noted that 16.9 % of grass-derived lignin and only 1.4 % hardwood-derived lignin were degraded to methane. Considering the large fraction of lignin that is not converted in anaerobic digestion, a further approach that could be employed to increase the overall value creation of second-generation bioethanol production is by means of pyrolysis of the digested stillage [10].

Fast pyrolysis is one of the thermochemical conversion processes which employs moderate temperatures (ca. 500 °C) with low vapor residence times (ca. 1–2 seconds) to devolatilize the feedstock in an oxygen-limited environment [11]. An international study led by Aston University in 2010 suggested that sulfur-free lignin (ALM Lignin) obtained from annually harvested non-woody plants (wheat straw and Sarkanda grass) cannot efficiently be fast pyrolysed. However, high-lignin feedstock with residual cellulose (ETEK lignin), similar to that derived in some bioethanol hydrolysis-based systems, is a more suitable feedstock for fast pyrolysis [12]. The main drawbacks were that (i) both types of lignin were prone to plugging in pneumatic or screw feeders if not cooled, (ii) agglomeration of lignin occured with inert materials in fluidised beds, (iii) low pyrolysis liquids yields were obtained, and (iv) very fine lignin particles (< 100 μm) could be carried through the reactor without decomposing, thus ending up in the pyrolysis liquids [12]. Nevertheless, with modifications for feeding, mixing, product collection and separation, lignin-rich feedstock such as digested stillage could potentially be processed by means of fast pyrolysis.

In this study, a mechanically stirred bed reactor with fractional condensation was used at different reaction temperatures to investigate fast pyrolysis of a novel substrate, being poplar-derived lignin-rich digested stillage. This study was aimed to assess the potential usage of lignin-rich digested stillage as fast pyrolysis feedstock. By combining anaerobic digestion of the stillage and fast pyrolysis of the digestate, an additional value to the bioethanol production chain could potentially be added. The process could have the potential to increase the overall value of second-generation bioethanol production by yielding valuable side-streams such as pyrolysis oils, phenolic compounds, non-condensable gases (NCG), and pyrolysis chars.

## 2. Materials and methods

### 2.1. Feedstock

Lignin-rich digested stillage was obtained from experiments concerned with bioethanol production from poplar at the Center for Microbial Ecology and Technology (CMET), Ghent University, Belgium and Bio-base Europe's Pilot Plant (Ghent, Belgium). The scheme in Fig. 1 shows how the fast-pyrolysis feedstock was produced.

The original feedstock for the second-generation bioethanol production was short rotation poplar wood, harvested in Lochristi

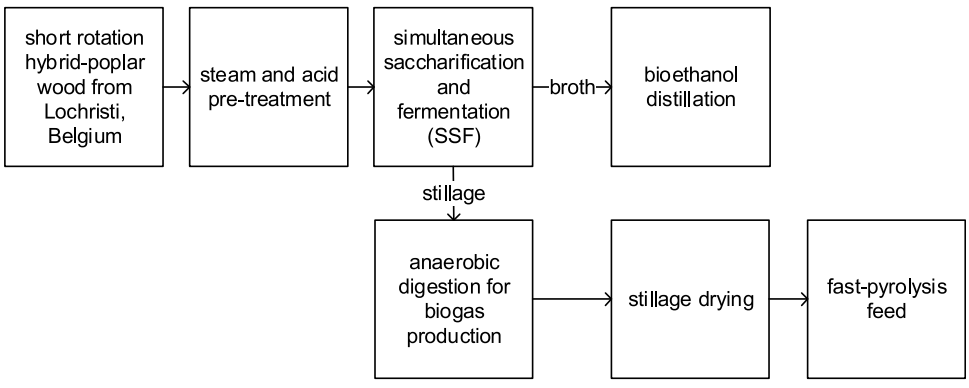


**Fig. 1.** Block flow diagram of the feedstock production.

(Belgium), and reduced in size to ± 1 cm chips. The chipped biomass was pre-steamed with bisulfite/sulfuric acid (ratio 4:1 in weight) at 170 °C for 30 min. A screw press and filter press were used to recover the solids, which were washed before fermentation. The pre-treated poplar was then subjected to simultaneous saccharification and fermentation (SSF) using ethanol yeast (Ethanol Red, Fermentis). The broth was distilled for bioethanol recovery, and the stillage was further processed for biogas production at 37 °C in a 53 l stainless steel reactor. A hydraulic retention time (HRT) of 39 ± 8 days and an average pH of 7.9 ± 0.2 was applied for biogas production.

The digestate, i.e. the slurry obtained after the anaerobic digestion was then dried (i.e. 24 h at 105 °C) and used as fast pyrolysis feedstock in the experiments of this study. The material was received in bulk dried form. The feedstock was milled and sieved to uniformly sized particles between 2–4 mm. Silica sand (PTB-Compaktuna, Gent, Belgium) with a particle density of 2650 kg $m^{-3}$ and mean diameter of 250 µm was used as the bed material in the mechanically stirred bed pyrolysis reactor.

### 2.2. Experimental setup

The fast pyrolysis experiments have been carried out in a setup involving a mechanically stirred bed reactor designed by the researchers of Department of Green Chemistry & Technology at Ghent University (Ghent, Belgium) and constructed by the University of Twente (Enschede, The Netherlands). The setup was first described by Yildiz et al. [13], the schematic drawing of the setup is shown in Fig. 2.

The fast pyrolysis reactor is equipped with a mechanical stirrer (4) providing an effective mixing of the bed contents (i.e. quartz sand and biomass). The nitrogen flow is utilized to displace the oxygen inside the reactor chamber at the beginning, and to convey the generated pyrolysis vapors through the exit of the reactor. The nitrogen flow rate was controlled at approximately 180 l $h^{-1}$ and fed from the bottom of the reactor. The feedstock was placed in a nitrogen gas purged chamber (3) to create an oxygen-free atmosphere and was then fed into the feeding screw (2). Every 10 min, the feedstock was fed from the purging chamber to the screw conveyer by manually handling the ball valves on top and at the bottom of the purging chamber. To ensure a smooth material flow and to avoid bridge formation, the purging chamber and the feeding hopper were pneumatically vibrated. As much as 96 g of the feedstock were fed into the reactor for each experiment in a one-hour time span, 16 g for each intermittent feeding every 10 min.

Fast pyrolysis at three different operating temperatures (430, 480 and 530 °C – temperature was selected based on the mass loss interval recorded in the TGA experiments as described later) each with five repetitions was carried out to determine the optimum fast pyrolysis temperature. Pyrolysis vapors that formed inside the reactor flowed through the heated knock-out vessel (6) which was maintained at 500 °C to capture solid particles that may have been entrained together with the gas flow. The high temperature in the knock-out vessel also prevented any condensation of pyrolysis vapors. Fractional condensation of pyrolysis liquids started when the hot pyrolysis vapors reached the electrostatic precipitator (ESP). The ESP wall temperature was maintained at 80 °C thus enabling simultaneous aerosol entrapment and condensation of pyrolysis vapors to form the heavy-phase pyrolysis liquids. Further condensation of the aqueous phase, including lighter and more volatile compounds took place in two, serially connected downstream tap-water cooled condensers. It was expected that all the heavy phase pyrolysis liquids would be condensed in the ESP collection flask, and the aqueous phase would be condensed in the tap-water cooled condenser flask, but in practice, small fractions of both phases were also found in both condensers. After each individual experiment, the liquids were collected both from the ESP collection flask and tap-water cooled condenser flasks (two flasks) and were consequently filtered and separated. The final unit of the system located before the gas flow meter was a cotton filter. This filter was necessary to minimise any residual solid particles and vapor droplets entering the gas flow meter so that only non-condensable gases (NCG) could pass through for volumetric flow measurement and off-line GC analysis. Reactor temperature, gas flow rates, and outlet gas temperature were monitored during each experiment. This experimental system was capable of measuring all the mass streams thus enabling the calculation of mass balances of solid, gas, and liquid product from fast pyrolysis.

Yields of each fast pyrolysis product (heavy and aqueous phases of the pyrolysis liquids, char, and NCG) were calculated on an as-received basis. Prior to and after each experiment, the ESP ($m_{ESP,i}$ and $m_{ESP,f}$), the glass condenser flasks ($m_{con,i}$ and $m_{con,f}$) and the cotton filter ($m_{f,i}$ and $m_{f,f}$) were weighed. The heavy phase yield $Y_{heavy}$ (in wt.%) calculation

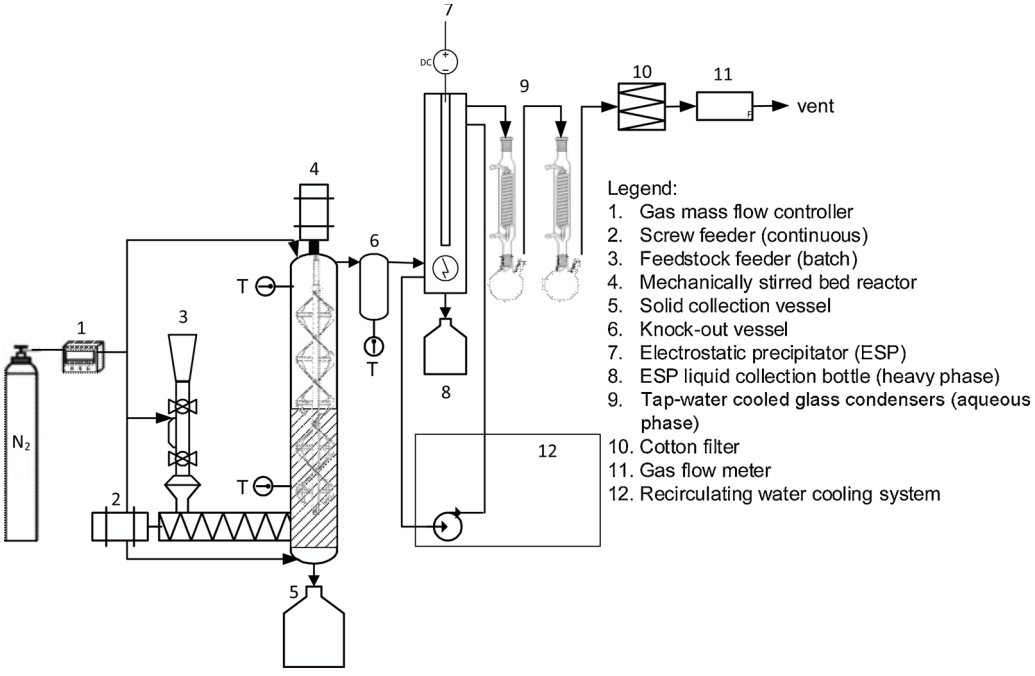


**Fig. 2.** Schematic drawing of the fast pyrolysis reactor and staged condensation system.

was quite straightforward and based on mass difference in the ESP while also the amount of heavy phase in the condenser flasks ($m_{h/a}$) and the residual aerosols in the cotton filter were added and the amount of aqueous phase in the ESP ($m_{a/h}$) was subtracted. As shown in Eq. (1), all this is finally divided by the feedstock mass ($m_{bm}$) and multiplied by one hundred to achieve a value in weight percentage. Similarly the aqueous phase yield ($Y_{aqueous}$ in wt.%) calculation was derived by determining the mass difference in the glass condenser flasks while also adding the amount of aqueous phase in the ESP ($m_{a,h}$) and subtracting the amount of heavy phase in the condenser flasks ($m_{h,a}$), see Eq. (2).

$$Y_{heavy} = [(m_{ESP,f} - m_{ESP,i}) + (m_{f,f} - m_{f,i}) + m_{h,a} - m_{a,h}] \cdot \frac{100}{m_{bm}} \quad (1)$$

$$Y_{aqueous} = [(m_{con,f} - m_{con,i}) + m_{a,h} - m_{h,a}] \cdot \frac{100}{m_{bm}} \quad (2)$$

The char yield ($Y_{char}$) was determined by subjecting the collected solids (char and fluidized bed material) to loss-on-ignition analysis which refers to the weight loss of a sample after ignition and combustion in air ($\Delta m_{loi}$) which is carried out in a muffle furnace (Carbolite AAF 1100) at 600 °C for minimum of 6 h. The total char yield is calculated based on the loss of mass after loss-on-ignition analyses compensated for the ash content ($A_c$ in wt.%), added by mass of the char in the heavy-phase pyrolysis liquids ($m_{c,h}$), mass of the char in the knockout vessel ($m_{c,k}$), and mass of char that was taken for sample analysis ($m_{c,rm}$).

$$Y_{char} = \left[ \left( \frac{\Delta m_{loi}}{100 - A_c} \right) + m_{c,h} + m_{c,k} + m_{c,rm} \right] \cdot \frac{100}{m_{bm}} \quad (3)$$

The non-condensable gas yield ($Y_{NCG}$) (Eq. (4)) was calculated based on the difference between the average volumetric gas flow rate during pyrolysis ($\bar{Q}_s$) at the outlet of the fast pyrolysis system and the average sweep gas ($N_2$) volumetric flow rate ($\bar{Q}_b$) introduced into the reactor. Conversion of volumetric flow rate to mass flow rate was done by determining the mixture gas density. Considering the non-ideal nature of pyrolysis gases, mixture gas densities were calculated using the Peng-Robinson equation of state based on the gas composition ($N_2$ free) as analyzed by the micro-GC and on the temperature at the outlet gas. The mixture gas density ($\rho_{NCG}$) calculation was performed using the Aspen® Hysis® software package.

$$Y_{NCG} = [(\bar{Q}_s - \bar{Q}_b) . t . \rho_{NCG}] \cdot \frac{100}{m_{bm}} \quad (4)$$

Mass balance closure ($Y_{tot}$ in wt.%) was defined as the sum of both pyrolysis liquid yields (both heavy and aqueous phases), char yield, and NCG yield:

$$Y_{tot} = Y_{heavy} + Y_{aqueous} + Y_{char} + Y_{NCG} \quad (5)$$

## 2.3. Analytical techniques

### 2.3.1. Energy content

The higher heating value (HHV) of pyrolysis liquids, char, and feedstock were determined using an E2K combustion calorimeter (Digital Data Systems, Gauteng, South Africa). The HHV of feedstock and chars were determined in accordance with ASTM D5468–02 ("Standard test method for gross calorific and ash value of waste materials") and ASTM D5865-13 ("Standard test method for the gross calorific value of coal and coke") using the same bomb calorimeter. The HHV of non-condensable gases was calculated using Aspen® Hysys® at known average gas outlet temperature and known gas composition based on gas chromatography (GC) results. Aspen® Hysys® calculates the HHV of non-condensable gases based on gas correlation methods and data from ISO 6976:1995 ("Calculation of calorific values, density, relative density and Wobbe index from the composition").

### 2.3.2. Moisture, ash, and lignin content

The quantification of moisture and ash in feedstock were respectively conducted in accordance to ASTM E871–82 ("Standard test method for moisture analysis of particulate wood fuels") and ASTM E1755–01 ("Standard test method for ash determination in biomass"). The acid-insoluble lignin fraction was determined according to the Technical Association of the Pulp and Paper Industry (TAPPI) T222 om-02 ("Acid-insoluble lignin in wood and pulp test") method by the Department of Plant Systems Biology, Flanders Institute of Biotechnology, Belgium. Regarding the pyrolysis solids content (i.e. entrained fine char particles) in pyrolysis liquids, this was determined using the filtration of solids in methanol method according to the ASTM D7579-09 ("Standard test method for pyrolysis solids content in pyrolysis liquids by filtration of solids in methanol"). The ash mass fraction of the chars ($A_c$ in wt.%) was calculated using Eq. (6), in which the ash mass fraction is calculated based on difference between the total mass fraction of carbon (), hydrogen ($w_H$), nitrogen ($w_N$), sulfur ($w_S$), and oxygen ($w_O$).

$$A_c = 100 - (w_C + w_H + w_N + w_S + w_O) \quad (6)$$

### 2.3.3. Thermogravimetric analysis (TGA)

Thermogravimetric analysis (TGA) of the feedstock was performed by the Department of Chemical Engineering, University of Groningen, The Netherlands. A TGA 7 from PerkinElmer was used for that. The samples were heated under a nitrogen atmosphere at a rate of 10 °C $min^{-1}$ from 20 °C until 900 °C.

### 2.3.4. Elemental composition analyses (TGA)

The elemental composition of the feedstock, chars, and pyrolysis liquids was determined by using a FLASH 2000 organic elemental analyser (Thermo Fisher Scientific, Waltham, USA) while applying the CHNS and oxygen configuration. The instrument was equipped with a thermal conductivity detector (TCD). 2,5-(Bis(5-tert-butyl-2-benzo-oxazol-2-yl) thiophene (BBOT) was used as standard. High purity helium (Alphagaz 1 from Air Liquide) was chosen as a carrier and reference gas. High purity oxygen (Alphagaz from Air Liquide) was chosen as combustion gas.

### 2.3.5. Non-condensable gases (NCG) analyses

The composition of the produced non-condensable gases (NCG) was determined off-line. Each gas sample was collected with a 100-ml gas-tight syringe and then analyzed on an Agilent Technologies 490 Micro GC. The micro GC was equipped with two TCD detectors and two analytical columns. The first column (10 m Molesieve 5A with back-flush) was set at 75 °C and its corresponding detector measured $H_2$, $N_2$, $CH_4$ and CO. The second column (10 m PPQ) was set to 70 °C and used for the determination of $CO_2$, $C_2H_4$, $C_2H_6$, $C_3H_6$ and $C_3H_8$. High purity argon and helium (Alphagaz 1 from Air Liquide) were used as the carrier gases.

### 2.3.6. Inductively coupled plasma optical emission spectrometry analyses

Inductively coupled plasma optical emission spectrometry (ICP-OES) for inorganic elemental analysis of both feedstock and pyrolysis char were performed by the Department of Chemical Engineering, University of Groningen, The Netherlands as described by Yin et al. [14]. ICP-OES was performed on a PerkinElmer 7000DV. Approximately 20 mg of solid sample was added to an aqueous solution of $HNO_3$ (8 ml, 65 wt.%). Prior to analyses, the samples were heat treated in a microwave oven. They were heated to 200 °C in 10 min, and then held at 200 °C for 15 min. Subsequently, $HNO_3$ solution (2 wt.% in water) was added to a total volume of 50 ml. The resulting solution was diluted ten times with deionised water.

*2.3.7. Pyrolysis liquids analyses (GCMS, GCxGC-FID, and 2D HSQC-NMR)*

The composition of the pyrolysis liquids was analysed in the first place using a standard GC-MS (Thermo Fisher Scientific Trace GC Ultra and Thermo ISQ MS). All the chromatogram analysis, integration, and adjustments were carried out with the help of data processing software (Xcalibur). Before injection into the GC-MS, the heavy phase of the pyrolysis liquid was diluted to a 20 wt.% solution in GC-grade tetrahydrofuran (Sigma-Aldrich) and spiked with 200 ppm of fluoranthene (Sigma-Aldrich) as an internal standard. The aqueous phase of the pyrolysis liquids was extracted using diethyl ether in 1:1 vol ratio and vigorously shaken for 5 min. Phase separation of the water phase and the solvent was further promoted by centrifugation at 13,000 rpm for 2 min. The extracted solvent phase was also spiked with 200 ppm of fluoranthene (Sigma-Aldrich) as an internal standard before injection into the GC-MS. Approximately 1 µl of a prepared sample was injected directly into the GC using a split/splitless injection port (split ratio 1:100) operated at 250 °C. The GC-MS used a Restek capillary column (Rtx-1701 crossbond with 14 % cyanopropylphenyl and 86 % dimethylpolysiloxane, 60 m in length, 0.25 mm internal diameter, and 0.25 µm film thickness) under constant helium carrier gas flow of 1 ml/min. The GC oven temperature program started with 3 min hold at 40 °C followed by heating to 280 °C at 5 °C $min^{-1}$. The final temperature was kept constant for 1 min. After the separation in the GC column, compounds were identified using an MS. The MS used 70 eV electron ionisation, and the mass selective detector scanned within an *m/z* range of 29–300. Quantification of peak area was obtained from integration of the total ion current (TIC) chromatogram. Identification of the individual components was performed by comparing their spectra with those found in the MS library from National Institute of Standards and Technology (NIST).

Additional GCxGC-FID and GPC analyses were performed by the Department of Chemical Engineering, University of Groningen, The Netherlands as described by Kloekhorst et al. [15] and Wildschut et al. [16]. The sample was analysed on a GCxGC-FID from Interscience equipped with a cryogenic trap system and two columns: a 30 m × 0.25 mm i.d. and a 0.25 µm film of RTX-1701 capillary column connected by a meltfit to a 120 cm × 0.15 mm i.d. and a 0.15 µm film Rxi-5Sil MS column. The GCxGC-FID was equipped with an FID detector and a dual jet modulator using liquid carbon dioxide to trap the samples. Helium was chosen as the carrier gas and continuously controlled at 0.6 ml $min^{-1}$. The injector temperature and FID temperature were set at 250 °C. The oven temperature was set at 40 °C for 5 min then heated up to 250 °C at a rate of 3 °C $min^{-1}$. The injector pressure was set at 70 kPa at 40 °C. The modulation time was 6 s.

The FID-response plot was analysed with GC Image® software. The identification of the primary GCxGC-FID component groups (e.g. alkanes, aromatics, alkylphenolics) in the pyrolysis liquids was made by spiking with representative model compounds for the component groups. Quantification was performed by using an average relative response factor (RRF) per component group with n-dibutyl ether (DBE) as the internal standard. Prior to GCxGC-FID analyses, the samples were diluted with an equal volume of tetrahydrofuran (THF) and finally, n-dibutyl ether (DBE) was added (to a concentration of 1 g $L^{-1}$) as an internal standard.

The heavy phase pyrolysis liquids were also analysed by 2D HSQC-NMR (two-dimensional (2D) $^{1}H$-$^{13}C$ heteronuclear single-quantum correlation nuclear magnetic resonance) at the Department of Chemical Engineering, University of Groningen, The Netherlands using methods described by Lancefield et al. [17]. A Bruker Ascend 700 MHz and 500 MHz spectrometer equipped with CPP TCI and CPP BBO probes respectively was used in these analyses. In each analysis, approximately 0.1 g of a heavy phase pyrolysis liquid sample was dissolved in 1 g of deuterated dimethyl sulfoxide (DMSO). Semi-quantitative 2D HSQC NMR analysis was performed using MestReNova 11.0.

*2.3.8. Molecular weight distribution of the heavy phase pyrolysis liquid analyses*

The molecular weight distribution of the heavy phase pyrolysis liquids was determined by Gel Permeation Chromatography (GPC). An HP1100 was used, equipped with three 300 × 7.5 mm PLgel 3 µm MIXED-E columns in series and a GBC LC1240 RI detector. Average molecular weight calculations were performed with the PSS WinGPC Unity® software from Polymer Standards Service. The following conditions were applied: THF as eluent at a flow rate of 1 ml $min^{-1}$, 140 bar, a column temperature of 42 °C, 20 µl injection volume and a 10 mg $ml^{-1}$ sample concentration. Toluene was used as a flow marker.

## 3. Results and discussion

### 3.1. Feedstock analyses

The characteristics of the lignin-rich digested stillage feedstock are summarised in Table 1. Even though the feedstock had a high ash content, the higher heating value of the feedstock was still considerable and it is just as energy dense as the non-treated poplar that was used in the second-generation bioethanol production. The HHV of the feedstock was approximately 20.6 MJ $kg^{-1}$ a.r. or 21.8 MJ $kg^{-1}$ d.b. while the HHV of hybrid poplar is typically around 18.4–19.6 MJ $kg^{-1}$ d.b. [18–20]. The acid-insoluble lignin content of the feedstock was approximately 63 wt.%, indicating that other poplar constituents were present (i.e. polysaccharides) and that the initial pre-treatment and enzymatic digestion of the poplar feedstock were still unable to convert and valorise all the cellulose and hemicellulose fractions from the feedstock.

From the results of ICP-OES (Table S1 in supplementary material section), it appears that the feedstock had a high concentration of alkaline earth metals, transition metals, and post-transitional metals, mainly aluminium, iron, and magnesium. Because of their catalytic effect in pyrolysis, the ash constituents can significantly alter the pyrolysis liquids composition and resulting physicochemical properties [21]. Inorganic salts/ash could catalyse specifically primary cellulose, hemicellulose, and (to a lesser extent) lignin pyrolysis reactions that enhance the formation of lower molecular weight species (especially formic and acetic acid, hydroxyacetaldehyde, and furan derivatives) [22,23]. Additionally, if inorganic salts/ash ends up in the pyrolysis oil, they promote the ageing of the fast pyrolysis oil.

Most of the ash will end up in the char and some of this char (3–8 % wt.% of the produced char) is transferred to the heavy phase. Leijenhorst et al. [24] suggest that transfer of metals to pyrolysis liquids is caused by solids (char) entrainment with the vapor stream as well as

**Table 1**
Lignin rich digested stillage feedstock characterization: moisture content (in wt.% a.r.), ash content (in wt.% d.b.), elemental composition (in wt.% d.b), and HHV (in MJ/kg a.r), Klason lignin content (in wt.% d.b). Standard deviations are given, BDL = below detection limit.

| Moisture | Ash | Ultimate analysis | | | | | HHV | Klason lignin |
|---|---|---|---|---|---|---|---|---|
| | | C | H | N | S | O | | |
| 5.7 ± 0.2 | 10 ± 0.1 | 50.2 ± 0.8 | 5.5 ± 0.0 | 2.7 ± 0.1 | BDL | 26.4 ± 1.5 | 20.6 ± 0.1 | 63.2 ± 0.7 |

volatilization of specific metal salts within the biomass. They also found that, on average, alkali metals are transferred for about 8 wt.% (based on total ash content) to the pyrolysis oil, while earth alkaline metals transfer for about 2 wt.% to the oil.

TGA-dTA analysis (Fig. 3) of the feedstock shows a thermal devolatilization pattern similar to those published previously for various types of lignin [25,26]. The feedstock mass loss already started at temperatures around 100 °C. This early mass loss must be due to evaporation of the water present in the feedstock (5.7 wt.%, see Table 1). Significant decomposition began to occur beyond a temperature of 200 °C. The high devolatilization rate in this temperature range of 200–400 °C is usually not assigned to the lignin thermal decomposition behavior [12], it is quite likely that the residual biomass constituents (i.e. polysaccharides) and microbial biomass (yeast cells from the ethanol fermentation as well as microbial biomass stemming from the anaerobic digestion) within the feedstock play a significant role in this type of pattern. Another factor could be that the lignin structure has been degraded already in the pretreatment process, *viz.* in such way the lignin has lost some of its thermal stability. At temperatures above 400 °C, the decomposition rate started to decrease until 900 °C where the remaining solid residue appeared to be approximately 25.5 wt.% on initial feedstock basis. Based on this thermal decomposition behavior, the most appropriate range of fast pyrolysis temperatures for lignin-rich digested stillage was predicted to be from 400 to 550 °C.

### 3.2. Fast pyrolysis product yields

Temperature plays a significant role in determining the yields of fast pyrolysis products. Table 2 summarises the product yields of lignin-rich digested stillage fast pyrolysis with varying reaction temperatures. Total (i.e. aqueous + heavy phase) pyrolysis liquid yields were quite similar at 430 °C and 480 °C. However, at the highest temperature (530 °C) tested, the aqueous phase yield increased to 13.4 wt.% while the heavy phase yield decreased to 15.1 wt.%.

Apparently, high temperatures were accelerating the dehydration reaction of the pyrolysis vapors, thus promoting the formation of higher amounts of the aqueous phase product. Observations on char and gas yield gave more distinct results regarding the effect of temperature in fast pyrolysis. At higher temperatures, further thermal cracking and devolatilization occurred, thereby augmenting gas production while reducing char formation. Gas production rose from 27.1 wt.% at 430 °C to 31.5 wt.% at 530 °C. The gas composition (Supplementary Table S2) also changed as a function of temperature: higher temperature promotes additional hydrogen, methane, and light hydrocarbons production. Blanco López et al. [27] and Uzun et al. [28] reported the same phenomenon during fast pyrolysis of olive stone and olive oil residue. Uzun et al. [28] proposed that the formation of $CH_4$ could be associated with the degradation of lignin, especially at higher temperatures as methane could be formed due to the release of methoxy groups on the phenolic rings in lignin which involves the rupture of the C—O bonds [28].

It is also noted that in order to avoid a high amount of entrained char in the pyrolysis liquids and to reduce the possibility of blockages, a fairly low $N_2$ volumetric flow rate of 160 l $h^{-1}$ was used – however still, prolonged experimental runs were difficult due to the buildup of char and coke at the reactor outlet. The low flow rate of nitrogen gas results in a pyrolysis vapor residence time, from the start of the devolatilization process until condensation being approximately 30 – 40 s. Such a long vapor residence time might have promoted further vapor-phase reactions, which may eventually have reduced the overall liquid yield.

### 3.3. Fast pyrolysis product characteristics

#### 3.3.1. Elemental composition

Ultimate analysis of each fast pyrolysis product is summarised in Table 3. At the higher temperature of 530 °C, carbonisation reactions intensified due to progressive char devolatilization and secondary pyrolysis vapor cracking leading to NCG production and char with less hydrogen. The heavy phase of the pyrolysis liquids also contained more carbon but slightly less hydrogen at elevated temperature.

Some of the phenolic compounds produced during fast pyrolysis of the lignin-rich digested stillage include both several high dew point (190 – 220 °C) compounds (e.g. alkyl phenols, methyl phenols, dimethyl phenols, and ethylphenol) and also low dew point (65 °C) phenols [29,30]. At higher temperature, thermal cracking of lignin components was accelerated, increasing the abundance of lower dew point phenols in the pyrolysis vapors. These low dew point phenols are more readily condensed in the second condenser (cooled with tap water). The collection of these lighter phenolics in the second condenser, rather than in the ESP reduces the oxygen content in the heavy phase which is collected underneath the ESP.

In the heavy phase pyrolysis liquids, a higher temperature further promotes oxygen removal, while increasing the carbon content. Compared to ordinary (non-phase separated) pyrolysis liquids from poplar or pine, heavy phase pyrolysis liquids obtained in this experiment contained less oxygen (11.3–13.36 wt.% compared to 35–40 wt.%), more carbon (59.9–62.83 wt.% compared to 54–58 wt.%) and more nitrogen (2–2.3 wt.% compared to 0–0.2 wt.%) [31,32]. The high nitrogen content can be linked to the presence of leftover yeast cells (from ethanol fermentation), leftover enzymes (from saccharification) and microbial biomass from anaerobic digestion in the feedstock. Even though the oxygen content is lower than in ordinary pyrolysis liquids from poplar or pine, a direct usage of the heavy phase for liquid fuel purposes is limited due to this high nitrogen content and relatively high oxygen content compared to petroleum-based fuels. Secondary upgrading by hydrotreatment is therefore still required [33].

#### 3.3.2. Energy content of fast pyrolysis products

Elemental composition of pyrolysis products correlates with their respective energy content. Higher carbon and hydrogen contents in the heavy phase increase the energy content up to 26.8–29.3 MJ $kg^{-1}$ (Table 4), significantly higher than the energy content of ordinary (non-phased separated) pine pyrolysis liquids (20–22 MJ $kg^{-1}$) [36]. The temperature of the fast pyrolysis process plays a role in densifying the energy within the pyrolysis liquids heavy phase: at higher temperatures, higher HHV heavy phase pyrolysis liquids were produced. The concentrations of highly energetic hydrogen and methane gases are increased with temperature, and on the contrary, low energetic gases (CO and $CO_2$) are decreased in concentration. As a consequence, higher temperatures increase the calculated HHV of the non-condensable gases.

#### 3.3.3. Redistribution of energy and elements within the pyrolytic products

Fast pyrolysis redistributes the energy and elemental make-up of the

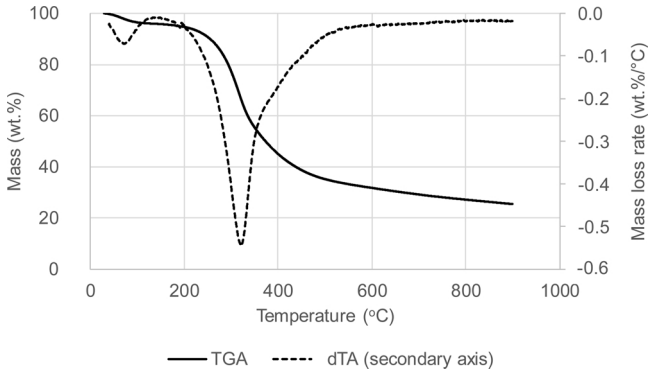


**Fig. 3.** TGA and dTA curves of digested stillage under $N_2$ flow at 10 °C $min^{-1}$ heating rate. The dTA curve was calculated from TGA data and smoothed using moving average.

**Table 2**
Fast pyrolysis product yield comparison at 430, 480 and 530 °C (in wt.%). Standard deviations are given.

| | Yields (wt.% on feed basis) | | |
|---|---|---|---|
| | 430 °C | 480 °C | 530 °C |
| Pyrolysis liquids | | | |
| Heavy Phase | 17.5 ± 3.7 | 18.1 ± 2.6 | 15.1 ± 2.1 |
| Aqueous Phase | 9.7 ± 3.7 | 9.9 ± 2.6 | 13.4 ± 2.1 |
| Pyrolytic char | 44.7 ± 3.5 | 39.5 ± 2.8 | 37.1 ± 1.4 |
| NCG | 27.1 ± 3.9 | 28.2 ± 2.1 | 31.5 ± 2.3 |
| Total | 99 ± 3.7 | 95.7 ± 2.5 | 97.1 ± 2 |

**Table 3**
Ultimate analysis of pyrolytic products produced at different temperatures (in wt.%, as produced). The oxygen concentration was determined directly, except for the aqueous phases in which it was determined by difference. Standard deviations are given.

| | Char | | |
|---|---|---|---|
| | 430 °C | 480 °C | 530 °C |
| N | 1.95 ± 0.13 | 2.26 ± 0.06 | 1.99 ± 0.04 |
| C | 59.86 ± 1.25 | 63.69 ± 0.34 | 62.83 ± 0.63 |
| H | 2.97 ± 0.08 | 2.99 ± 0.09 | 2.24 ± 0.02 |
| S | Below LOD | Below LOD | Below LOD |
| O | 13.36 ± 1.14 | 9.93 ± 0.06 | 11.28 ± 0.20 |
| Ash | 21.87 ± 0.85 | 21.12 ± 0.18 | 21.66 ± 0.33 |
| | Heavy phase | | |
| | 430 °C | 480 °C | 530 °C |
| N | 4.01 ± 0.09 | 4.52 ± 0.09 | 5.54 ± 0.06 |
| C | 62.09 ± 0.22 | 64.8 ± 0.64 | 66.60 ± 0.40 |
| H | 7.79 ± 0.10 | 7.74 ± 0.06 | 7.27 ± 0.06 |
| S | Below LOD | Below LOD | Below LOD |
| O | 21.19 ± 3.21 | 17.39 ± 0.28 | 17.86 ± 0.35 |
| | Aqueous phase | | |
| | 430 °C | 480 °C | 530 °C |
| N | 1.73 ± 0.07 | 1.58 ± 0.11 | 1.63 ± 0.07 |
| C | 4.73 ± 0.06 | 3.69 ± 0.17 | 3.33 ± 0.04 |
| H | 11.16 ± 0.06 | 10.42 ± 0.88 | 11.07 ± 0.11 |
| S | 0.19 ± 0.03 | 0.13 ± 0.01 | 0.12 ± 0.01 |
| O | 82.19 ± 0.06 | 84.18 ± 0.45 | 83.85 ± 0.07 |

**Table 4**
HHV (bomb calorimetry) of pyrolytic products produced at different temperature (in MJ $kg^{-1}$, as produced). Standard deviations are given, except for NCG for which the HHV was computed based on known gas concentrations.

| | 430 °C | 480 °C | 530 °C |
|---|---|---|---|
| Heavy phase liquid | 26.8 ± 0.6 | 27.2 ± 0.8 | 29.3 ± 0.2 |
| Char | 22.2 ± 0.0 | 23.9 ± 0.5 | 23.5 ± 1.3 |
| Gas ($N_2$-free) at 30 °C | 7.6 | 6.9 | 11.8 |

feedstock to the resulting products. The distribution of the initial feedstock energy to fast pyrolysis products (char, gases, and heavy phase pyrolysis liquid – aqueous phase was omitted as no HHV was measured therein) were not significantly different at each pyrolysis temperature (Supplementary Figure S1). But there is one exception: at the highest fast pyrolysis temperature (530 °C), slightly more feedstock energy ends up in the non-condensable gases. The latter can be explained by a combination of higher gas yield and the NCG's having a higher energy content (due to larger methane and light hydrocarbon concentrations) at 530 °C.

The elemental distribution of fast pyrolysis products is shown in Table S3. These numbers were calculated from the product yield and the elemental content of the individual pyrolytic products. An element with a high abundance (based on elemental analysis results) in one of the pyrolysis product might have low distribution value if the product yield was low. The redistribution of feedstock carbon and hydrogen was mostly equal among heavy and aqueous phases regardless of the pyrolysis temperature. At the higher temperature of 530 °C, the carbon content of char (Table 3) was the highest, but the product yield (Table 2) was the lowest. While considering the product of these two, the redistribution of feedstock carbon in char (Supplementary Table S4) appears to decrease with the temperature. The same occurred for hydrogen in char, which appeared to decrease with temperature as well. That again is caused by the lower char yield and lower hydrogen content of the char at higher temperatures (Tables 2 and 3).

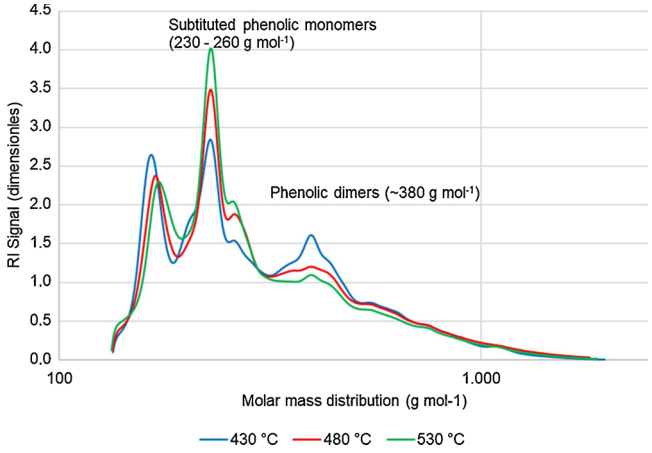


**Fig. 4.** Gel permeation chromatograms comparison of heavy phase pyrolysis liquids produced at different fast pyrolysis temperatures, logarithmic scale.

### 3.3.4. GPC analysis

Fig. 4 shows the molar mass distribution (in logarithmic scale) and Supplementary Table S4 shows the weight-average molecular weight ($M_w$) and the number-average molecular weight ($M_n$) for the heavy phase pyrolysis liquids produced from the feedstock at different temperatures.

The $M_n$ for all the pyrolysis liquids sample were ranging between 263–270 g $mol^{-1}$ and the $M_w$ ranged between 342–357 g $mol^{-1}$. The $M_n$ and $M_w$ value suggest that the heavy phase pyrolysis liquids mostly consisted of medium to high molecular weight compounds. The effect of fast pyrolysis temperature was profoundly visible in the GPC profile at specific molar mass ranges. The depolymerisation of lignin during fast pyrolysis mainly occurred via the cleavage of $\beta$-O-4 bonds in the lignin structure and thermal ejection of lignin oligomers into aerosols both of which were accelerated by higher temperatures [34,35]. Patwardhan et al. [36] conducted a comprehensive GPC analysis of pyrolysis liquids from lignin derived from corn stover. In this study, it was found that the lignin-derived pyrolysis liquids contain mostly phenolic monomers (212 Da, including substituted phenols) and oligomeric phenols in the form of dimers (432 Da), trimers (662 Da), and tetra-pentamers (1168 Da). In the current study, GPC analysis shows that fast pyrolysis of the feedstock will produce both phenolic monomers and phenolic dimers, but at higher temperatures (i.e. 530 °C) more phenolic monomers (230 – 260 g $mol^{-1}$ range) were produced, and less phenolic dimers (~380 g $mol^{-1}$ range). The higher fast pyrolysis temperature also increases the cracking reaction rate of phenolic dimers into phenolic monomers.

### 3.3.5. GC–MS and GCxGC-FID analysis

Due to the nature of the feedstock composition, heavy phase pyrolysis liquids contain various pyrolytic components derived from a

combination of residual poplar polysaccharides (e.g. hemicellulose), microbial biomass and lignin. Supplementary Figure S2 summarises the relative quantification (in peak area %) of primary key components determined by GC–MS. GC–MS and GCxGC-FID could not quantify all the components in the heavy phase pyrolysis liquids. According to our calculation using the GCxGC-FID data, only 16 – 26 wt.% of all heavy phase components are volatile and GC-detectable compounds, with the remainder likely being heavier and high-boiling compounds (e.g. phenolic dimers).

Compounds like 2-furanmethanol, 3-methyl-2-cyclopentene-1-one, 1,4:3,6-dianhydro-α-D-glucopyranose and acetic acid are most probably degradation products from cellulose or hemicelluloses and were found in the heavy phase pyrolysis liquids at every temperature tested, although in relatively small amounts. Their presence indicates that there are still polysaccharide compounds present in the digested lignin stillage which are neither consumed in the ethanol fermentation nor in the subsequent anaerobic digestion. A significant portion of the heavy phase pyrolysis liquid contains numerous phenolic compounds. Phenolic monomers (including substituted phenols) such as phenol, *o*-cresol, and *m*-cresol had the highest relative area percentage as shown in Supplementary Figure S2. It is also worth mentioning that only 75–83 % peak area of THF-soluble volatile compounds could be identified.

Fig. 5 shows GCxGC FID chromatograms of heavy phase pyrolysis liquids produced at different fast pyrolysis temperatures with a division of the 2D chromatogram into regions according to chemical functionalities. Region 1 is mainly cyclic alkanes, region 2 is primarily linear/branched alkanes, region 3 and 4 are aromatics (including polycyclic aromatic hydrocarbons), region 5 and 6 are ketones, alcohols, and acids, region 7 and 8 are phenols and phenolic compounds. Also “a” is internal standard, and “b” is butylated hydroxytoluene (stabilizer in THF).

Further quantification of the GCxGC FID results from Fig. 5 is provided in Table 5. Higher temperatures promoted further formation of dihydroxybenzenes, naphthalenes, and an increase in phenols was expected from further degradation of lignin monomers of the feedstock. Unconjugated alkenes found in the heavy phase pyrolysis liquid are most likely originating from residual microbial biomass left after anaerobic digestion (i.e. resulting from the pyrolysis of unsaturated fatty acids). The highest concentration of unconjugated alkenes, hydrocarbons, and ketones is achieved at a fast pyrolysis temperature of 480 °C. Even at a lower temperature (i.e. 430 °C), the feedstock could produce unconjugated alkenes, hydrocarbons, and ketones. Higher fast pyrolysis temperatures (i.e. 530 °C) will accelerate further reactions of unconjugated alkenes, hydrocarbons, and ketones to be broken down into smaller components (e.g. short chain hydrocarbons and light oxygenates). This effect is also significantly observable in the methoxyphenols concentration which decreased as the temperature increased. This result could be attributed to either enhanced demethoxylation at higher temperatures [35] or combined demethylation-dehydroxylation in the presence of catalyzing metals [37] which were abundantly present in the ash of the feedstock.

Some lighter and water-soluble compounds can be detected in the aqueous phase of the pyrolysis liquids. Liquid-liquid extraction with diethyl ether was not fully effective in extracting all the water-soluble pyrolysis liquid components from the aqueous phase. Only non-polar compounds with a high affinity to the solvent could be extracted. GC–MS relative quantification of extracted aqueous phase is summarised in Table 6. Most of the THF-soluble compounds are phenols, phenolic monomers, 2-furanmethanol, pyrrole, and 1,2-benzenediol.

### 3.3.6. D HSQC NMR analysis

Fig. 6 shows three 2D HSQC NMR graphs of heavy phase pyrolysis liquids produced from fast pyrolysis of the feedstock at a different temperature. The area percentage of the 2D HSQC NMR peaks are shown in Figure S3.

Due to the complexity of the heavy phase pyrolysis liquids, it is difficult to obtain high-resolution peaks with distinct separation of the chemical shift to accurately pinpoint the detailed structures of the chemical components of the pyrolysis liquids constituents. HSQC 2D NMR results and subsequence relative integration values confirm our previous discussions that higher temperature does play a significant role in determining the chemical composition of pyrolysis liquids. All the heavy phase pyrolysis liquids from the feedstock contained three main phenolic phenylpropanoids (S, G, H unit derived) compounds, pyrolytic sugars, aliphatics, aliphatics with aromatic groups, and unconjugated alkenes, and aligned with other 2D HSQC NMR analysis using lignin-rich feed and lignin-rich derived pyrolysis oils [17,38]. It is highly probable that pyrolytic sugars originated from hemicellulose or cellulose while the unconjugated alkenes were derived from residual microbial biomass (e.g. lipid components). At higher temperatures, the most significant changes were the diminishing of methoxy groups (-O-Me) and the increase in phenolic and aliphatic groups. The reduction of area percentage of -O-Me group was also coupled with a decrease in area percentage of the S-unit phenylpropanoids; this suggests that the -O-Me chains in the S-unit phenylpropanoid is very susceptible to thermal degradation and the reaction is enhanced at higher vapor residence time in the setup. The total aliphatic groups and heteroatom-aliphatic abundance were also greatly affected by the increasing temperature. Higher temperature promotes aliphatic formation due to the

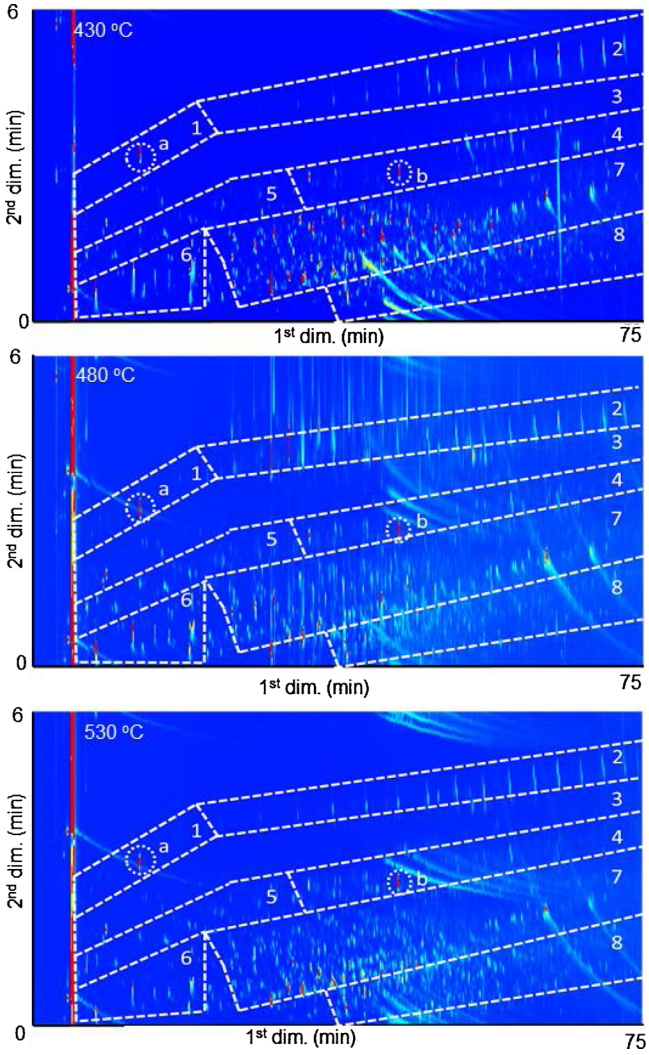


**Fig. 5.** GCxGC FID chromatogram of heavy phase pyrolysis liquids produced at 430, 480 and 530 °C.

**Table 5**
GCxGC FID quantification (in wt.%) of chemicals groups found in heavy phase pyrolysis liquids.

| Group Type | 430 °C | 480 °C | 530 °C |
|---|---|---|---|
| Aromatics | 0.31 | 0.64 | 0.4 |
| Cycloalkanes | < 0.01 | 0.05 | 0.02 |
| Dihydroxybenzenes | 5.37 | 2.32 | 7.42 |
| Hydrocarbons | 0.89 | 1.43 | 0.61 |
| Ketones, acids, and alcohols | 4.37 | 4.01 | 4.76 |
| Methoxyphenols | 5.45 | 1.51 | 1.05 |
| Naphthalenes | 0.36 | 0.54 | 0.78 |
| Phenols | 7.7 | 5.62 | 11.82 |
| Volatile fraction quantified | 24.46 | 16.11 | 26.87 |

**Table 6**
Key chemical compounds found in extracted water phases produced at different pyrolysis temperatures (relative abundance expressed in solvent-free peak area %).

| | 430 °C | 480 °C | 530 °C |
|---|---|---|---|
| Acetic acid | 0.24 | 1.37 | 0.43 |
| Pyrrole | 2.04 | 2.79 | 5.01 |
| 2-Furanmethanol | 3.94 | 1.96 | 0.90 |
| Phenol | 36.30 | 56.49 | 68.69 |
| Guaiacol | 26.30 | 8.43 | 1.69 |
| *o*-Cresol | 1.51 | 6.37 | 9.07 |
| *m*-Cresol | 2.42 | 5.13 | 9.73 |
| 1,2-Benzenediol | 2.66 | 11.26 | 4.48 |

increase in primary lignin cracking reactions.

### 3.4. Fast pyrolysis reaction pathway

Based on the analysis of the heavy phase pyrolysis liquids, we could draw the main reactions pathway during fast pyrolysis of the feedstock. The proposed pathway (Fig. 7) was based on the assumption that the residual polysaccharide components in the feedstock were derived from hemicellulose, cellulose or both, and the reaction pathways from residual microbial biomass were omitted due to the lack of additional detailed analysis. The hemicellulose part underwent ring scission, and rearrangement reactions yielding in carboxylic acids and dehydration reaction resulting in furan compounds and water [39–41]. Both reactions were positively influenced by increasing temperature, hence the increased water yield and 2-furanmethanol relative area percentage at higher fast pyrolysis temperature.

The lignin part was more complicated, and the proposed pathway may not be able to map all the actual reactions of lignin during fast pyrolysis. Two main hypotheses regarding the main reaction during fast pyrolysis of lignin were primary cracking - depolymerisation and thermal ejection. Primary cracking of lignin produced phenols and substituted phenols, while thermal ejection produced more phenolic oligomers (e.g. phenolic dimers) [42]. Thermal ejection, primary cracking of the lignin polymer, and depolymerisation reaction of phenolic dimers were greatly enhanced by higher temperature marked by the increased concentration of phenols and methoxyphenol quantified by GCxGC FID. There was no apparent result to suggest that dimerisation reaction occurred and were influenced by temperature.

Two main subsequent possible reactions occurred with methoxyphenols; both were enhanced by a metal catalyst. Most probably the ash content (e.g. Fe, Mn, and Ni) of the feedstock could catalyse these types of reactions. One of the reaction was a combination of demethylation reactions which produces catechol, methane, and methyl-substituted ring products (e.g. toluene and cresol) [43]. Toluene and cresol were found in the heavy phase pyrolysis liquids (based on GC–MS) but not catechol. The second reaction that might have occurred was demethoxylation of methoxyphenol into phenols and alcohol

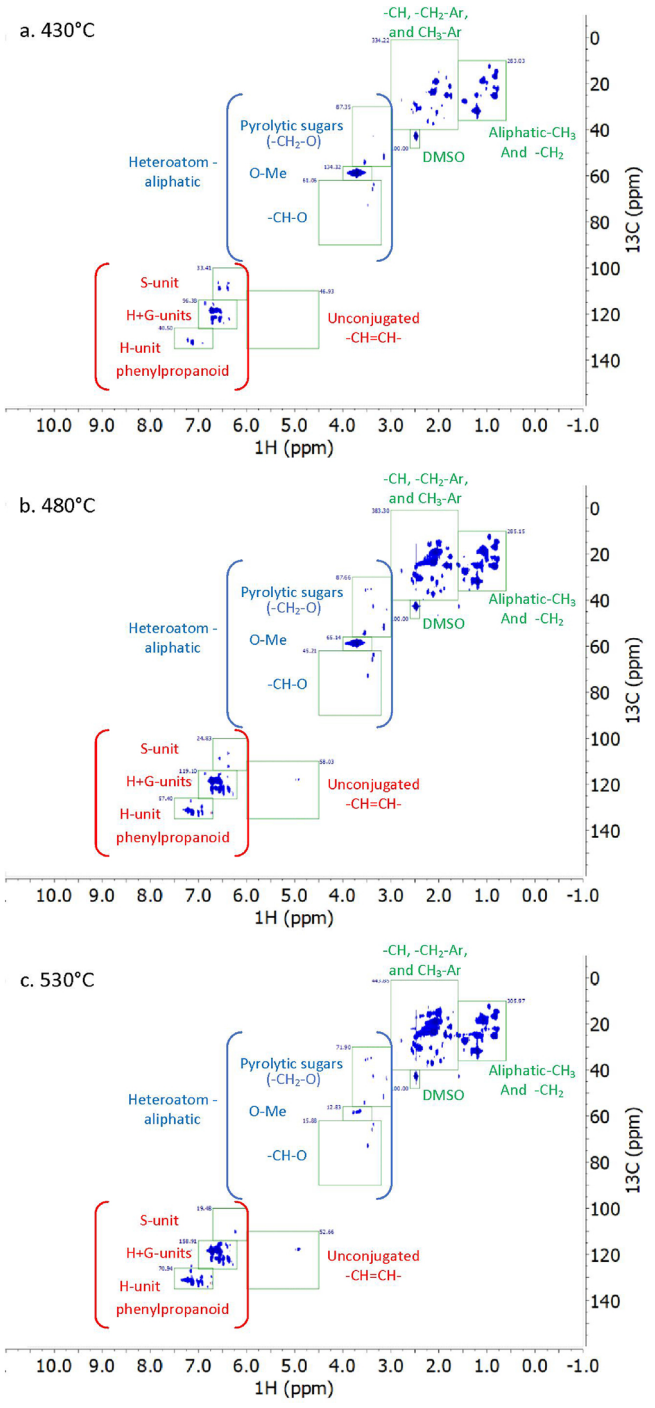


**Fig. 6.** 2D HSQC NMR analysis and assignment of heavy phase pyrolysis liquid functional groups.

groups (e.g. methanol) which could be confirmed by the decrease in the -O-Me linkage found by 2D HSQC NMR [37].

Phenols might be further converted into monocyclic aromatic hydrocarbon (MAHs) (e.g. benzene, toluene) which then will be further converted into polycyclic aromatic hydrocarbon (PAHs) (e.g. naphthalene). Increasing the fast pyrolysis temperature enhanced both reactions, and the conversion of MAH to PAH, which is catalysed by carboxylic acids [41].

Pyrolysis char production mostly comes from both hemicellulose and lignin. High fast pyrolysis temperatures promote carbonisation reactions which produce char with a high carbon content together with hydrogen gas. The phenomenon was confirmed by the production of

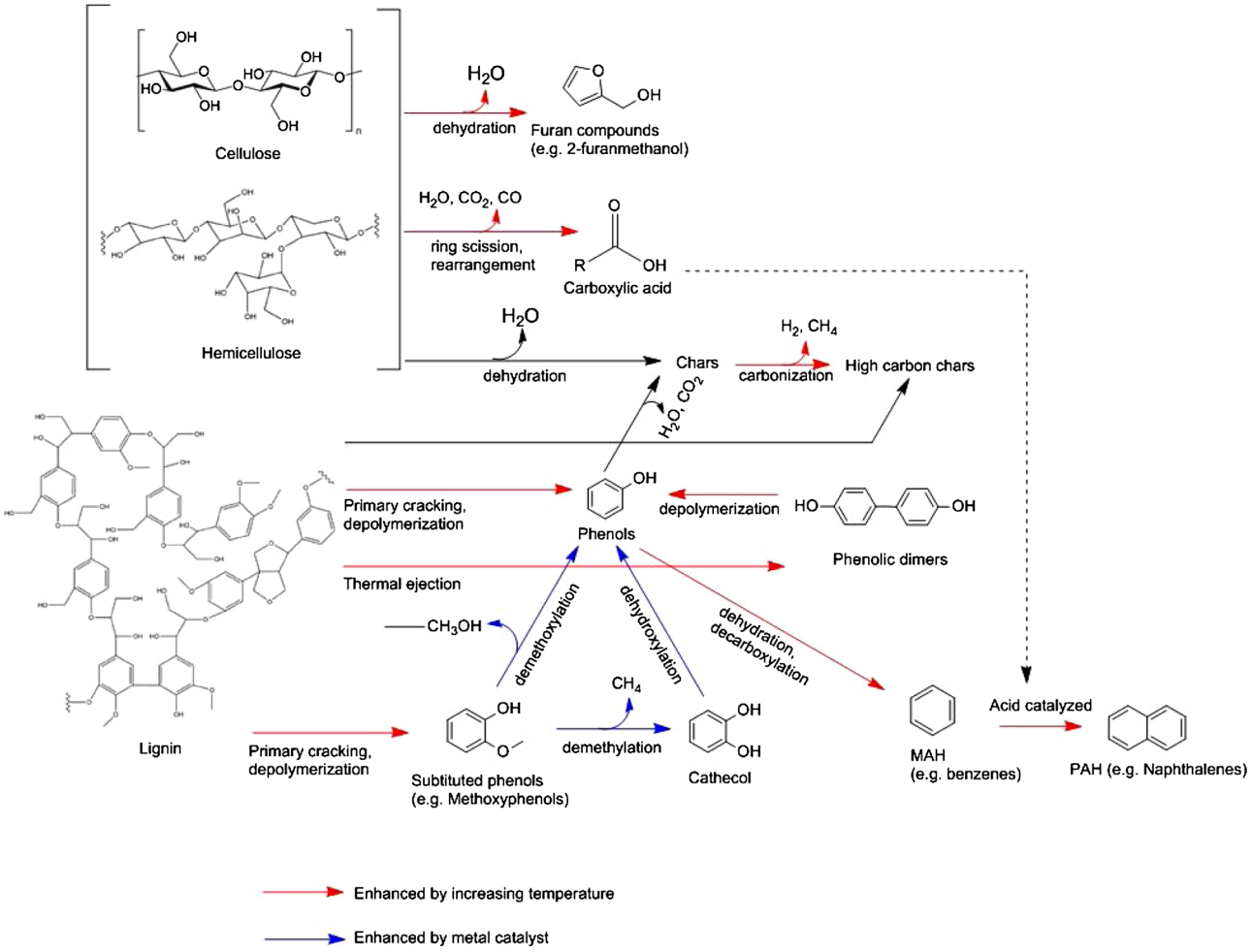


**Fig. 7.** Proposed main reactions during fast pyrolysis of the feedstock. Red line indicates reactions that were augmented by increasing temperature. The blue line indicated reactions that were enhanced by metal catalysts (present in the ash). Scheme constructed from previously published suggestions [13,39–42].

char with high a carbon content (based on elemental analysis).

### *3.5. Contribution of fast pyrolysis toward the complete process of a second-generation bioethanol biorefinery*

The contribution of fast pyrolysis of the lignin-rich digested stillage to the value chain of a second-generation bioethanol production is shown in the scheme of Supplementary Figure S4. The scope of the yield calculation was the solid yield from Simultaneous Saccharification and Fermentation (SSF), followed by anaerobic digestion because fast pyrolysis will only add additional value to those solid residues. All the data on SSF and anaerobic digestion were taken from Coma et al. [44]

Pretreatment and SSF of the initial feedstock resulted in about, 34.2 wt.% (on poplar feedstock basis) residual solids available for the anaerobic digestion process. After anaerobic digestion, the residual solids were reduced to 21.6 wt.% (expressed on feedstock weight basis), with an additional quantity of 9.65 wt.% of volatile solids.

Out of this total of 31.3 wt.% (expressed on feedstock weight basis), fast pyrolysis (at 480 °C) could valorize around 85.8 % of the mass of incoming feedstock (i.e. dry digestate at this point) under the assumption that pyrolysis char and NCGs were considered as useful products as well. The contribution of fast pyrolysis towards the complete process of a second-generation bioethanol production, in terms of additional solid residue out of the whole feedstock being valorized, was around 26.8 wt.% with only 4.5 wt.% (aqueous phase product, on feedstock basis) being considered as a low-value product.

## 4. Conclusions

A mechanically stirred bed reactor with fractional condensation was used at different reaction temperatures to investigate the outcomes of fast pyrolysis of a novel feedstock. The feedstock consisted of a lignin-rich residue that is obtained after lignocellulosic ethanol production, followed by anaerobic digestion of the stillage. Given the high lignin content of the feedstock, in this type of setup no technical issues (i.e. plugging, bed agglomeration, etc…) were encountered during fast pyrolysis. The heavy phase pyrolysis liquid, aqueous phase, pyrolysis char and NCGs yield were consecutively between 15.1–18.1 wt.%, 9.7–13.4 wt.%, 37.1–44.7 wt.% and 27.1–31.5 wt.% (a.r. feedstock based). Higher pyrolysis temperatures promote primary depolymerisation and dehydration reactions while reducing char formation. However, these higher temperatures will be off-set by a higher tendency for secondary reactions, hence the importance to keep vapor residence time to a minimum. The heavy phase pyrolysis liquid, char and NCG were found to be favorable candidates for use as fuels, though the relatively high nitrogen content in the heavy pyrolysis liquid as well as the high ash content in the char require further attention, as they may pose specific issues during combustion. For the char, alternative uses such as in soil amendment or as absorbent may be foreseen if combustion is not favorable. Fast pyrolysis was able to contribute to an increase of 26.8 wt.% of additional conversion of otherwise unused solid residues, thus enhancing the overall value creation in lignocellulosic ethanol production.

## CRediT authorship contribution statement

**Neil Priharto:** Methodology, Investigation, Formal analysis, Writing - original draft. **Frederik Ronsse:** Writing - review & editing, Supervision, Resources. **Güray Yildiz:** Methodology, Formal analysis. **Hero Jan Heeres:** Supervision, Resources, Writing - review & editing. **Peter J. Deuss:** Investigation, Formal analysis. **Wolter Prins:** Conceptualization, Writing - review & editing, Supervision, Project administration.

## Acknowledgements

The authors would like to acknowledge the following colleagues for their significant contribution:

## Appendix A. Supplementary data

Supplementary material related to this article can be found, in the online version, at doi:https://doi.org/10.1016/j.jaap.2019.104756.

## References

[1] A. Mohr, S. Raman, Lessons from first generation biofuels and implications for the sustainability appraisal of second generation biofuels, Energy Policy 63 (2013) 114–122, https://doi.org/10.1016/j.enpol.2013.08.033.
[2] R. Lal, Biofuels and carbon offsets, Biofuels 5 (2014) 21–27, https://doi.org/10.4155/bfs.13.62.
[3] T.W. Hudiburg, W. Wang, M. Khanna, S.P. Long, P. Dwivedi, W.J. Parton, M. Hartman, E.H. Delucia, Impacts of a 32-billion-gallon bioenergy landscape on land and fossil fuel use in the US, Nat. Energy 1 (2016) 1–7, https://doi.org/10.1038/nenergy.2015.5.
[4] J. Littlewood, M. Guo, W. Boerjan, R.J. Murphy, Bioethanol from poplar: a commercially viable alternative to fossil fuel in the European Union, Biotechnol. Biofuels 7 (2014) 113, https://doi.org/10.1186/1754-6834-7-113.
[5] M.J. Negro, P. Manzanares, I. Ballesteros, J.M. Oliva, A. Cabañas, M. Ballesteros, Hydrothermal pretreatment conditions to enhance ethanol production from poplar biomass, Appl. Biochem. Biotechnol. 105 (2003) 87–100, https://doi.org/10.1385/ABAB:105:1-3:87.
[6] C. Kundu, H.J. Lee, J.W. Lee, Enhanced bioethanol production from yellow poplar by deacetylation and oxalic acid pretreatment without detoxification, Bioresour. Technol. 178 (2015) 28–35, https://doi.org/10.1016/j.biortech.2014.08.082.
[7] A. Barakat, F. Monlau, J.P. Steyer, H. Carrere, Effect of lignin-derived and furan compounds found in lignocellulosic hydrolysates on biomethane production, Bioresour. Technol. 104 (2012) 90–99, https://doi.org/10.1016/j.biortech.2011.10.060.
[8] M. Koyama, S. Yamamoto, K. Ishikawa, S. Ban, T. Toda, Enhancing anaerobic digestibility of lignin-rich submerged macrophyte using thermochemical pre-treatment, Biochem. Eng. J. 99 (2015) 124–130, https://doi.org/10.1016/j.bej.2015.03.013.
[9] R. Benner, A.E. Maccubbin, R.E. Hodson, Anaerobic biodegradation of the lignin and polysaccharide components of Lignocellulose and synthetic lignin by sediment microflora, Appl. Envir. Microbiol. 47 (1984) 998–1004, https://doi.org/10.3354/meps023221.
[10] S. Ghysels, F. Ronsse, D. Dickinson, W. Prins, Production and characterization of slow pyrolysis biochar from lignin-rich digested stillage from lignocellulosic ethanol production, Biomass Bioenergy 122 (2019) 349–360, https://doi.org/10.1016/j.biombioe.2019.01.040.
[11] A.V. Bridgwater, Review of fast pyrolysis of biomass and product upgrading, Biomass Bioenergy 38 (2012) 68–94, https://doi.org/10.1016/j.biombioe.2011.01.048.
[12] D.J. Nowakowski, A.V. Bridgwater, D.C. Elliott, D. Meier, P. de Wild, Lignin fast pyrolysis: results from an international collaboration, J. Anal. Appl. Pyrolysis 88 (2010) 53–72, https://doi.org/10.1016/j.jaap.2010.02.009.
[13] G. Yildiz, T. Lathouwers, H.E. Toraman, K.M. Van Geem, G.B. Marin, F. Ronsse, R. Van Duren, S.R.A. Kersten, W. Prins, Catalytic fast pyrolysis of pine wood: effect of successive catalyst regeneration, Energy Fuels 28 (2014) 4560–4572, https://doi.org/10.1021/ef500636c.
[14] W. Yin, R.H. Venderbosch, G. Bottari, K.K. Krawzcyk, K. Barta, H.J. Heeres, Catalytic upgrading of sugar fractions from pyrolysis oils in supercritical monoalcohols over Cu doped porous metal oxide, Appl. Catal. B Environ. 166–167 (2015) 56–65, https://doi.org/10.1016/j.apcatb.2014.10.065.
[15] A. Kloekhorst, J. Wildschut, H.J. Heeres, Catalytic hydrotreatment of pyrolytic lignins to give alkylphenolics and aromatics using a supported Ru catalyst, Catal. Sci. Technol. 4 (2014) 2367–2377, https://doi.org/10.1039/C4CY00242C.
[16] J.H. Marsman, J. Wildschut, F. Mahfud, H.J. Heeres, Identification of components in fast pyrolysis oil and upgraded products by comprehensive two-dimensional gas chromatography and flame ionisation detection, J. Chromatogr. A 1150 (2007) 21–27, https://doi.org/10.1016/j.chroma.2006.11.047.
[17] C.W. Lahive, P.J. Deuss, C.S. Lance, Z. Sun, D.B. Cordes, C.M. Young, F. Tran, A.M.Z. Slawin, J.G. De Vries, P.C.J. Kamer, N.J. Westwood, K. Barta, Advanced Model Compounds for Understanding Acid-catalyzed Lignin Depolymerization: Identification of Renewable Aromatics and a Lignin-derived Solvent, (2016), https://doi.org/10.1021/jacs.6b04144.
[18] F.A. Agblevor, S. Beis, O. Mante, N. Abdoulmoumine, Fractional catalytic pyrolysis of hybrid poplar wood, Ind. Eng. Chem. Res. 49 (2010) 3533–3538, https://doi.org/10.1021/ie901629r.
[19] M. Sabatti, F. Fabbrini, A. Harfouche, I. Beritognolo, L. Mareschi, M. Carlini, P. Paris, G. Scarascia-Mugnozza, Evaluation of biomass production potential and heating value of hybrid poplar genotypes in a short-rotation culture in Italy, Ind. Crops Prod. 61 (2014) 62–73, https://doi.org/10.1016/j.indcrop.2014.06.043.
[20] M.S. Verlinden, L.S. Broeckx, J. Van den Bulcke, J. Van Acker, R. Ceulemans, Comparative study of biomass determinants of 12 poplar (Populus) genotypes in a high-density short-rotation culture, For. Ecol. Manage. 307 (2013) 101–111, https://doi.org/10.1016/j.foreco.2013.06.062.
[21] G. Yildiz, F. Ronsse, R. Venderbosch, R. van Duren, S.R.A. Kersten, W. Prins, Effect of biomass ash in catalytic fast pyrolysis of pine wood, Appl. Catal. B Environ. 168–169 (2015) 203–211, https://doi.org/10.1016/j.apcatb.2014.12.044.
[22] P.R. Patwardhan, J.A. Satrio, R.C. Brown, B.H. Shanks, Influence of inorganic salts on the primary pyrolysis products of cellulose, Bioresour. Technol. 101 (2010) 4646–4655, https://doi.org/10.1016/j.biortech.2010.01.112.
[23] A. Oasmaa, B. Van De Beld, P. Saari, D.C. Elliott, Y. Solantausta, Norms, standards, and legislation for fast pyrolysis bio-oils from lignocellulosic biomass, Energy Fuels 29 (2015) 2471–2484, https://doi.org/10.1021/acs.energyfuels.5b00026.
[24] E.J. Leijenhorst, L. van de Beld, E. Meers, W. Prins, Fate of Minerals in the Fast Pyrolysis Process, (2014), https://doi.org/10.13140/RG.2.1.1811.3364.
[25] G. Jiang, D.J. Nowakowski, A.V. Bridgwater, A systematic study of the kinetics of lignin pyrolysis, Thermochim. Acta 498 (2010) 61–66, https://doi.org/10.1016/j.tca.2009.10.003.
[26] H. Yang, R. Yan, H. Chen, D.H. Lee, C. Zheng, Characteristics of hemicellulose, cellulose and lignin pyrolysis, Fuel 86 (2007) 1781–1788, https://doi.org/10.1016/j.fuel.2006.12.013.
[27] M.C. Blanco López, C.G. Blanco, A. Martínez-Alonso, J.M.D. Tascón, Composition of gases released during olive stones pyrolysis, J. Anal. Appl. Pyrolysis 65 (2002) 313–322, https://doi.org/10.1016/S0165-2370(02)00008-6.
[28] B.B. Uzun, A.E. Pütün, E. Pütün, Composition of products obtained via fast pyrolysis of olive-oil residue: effect of pyrolysis temperature, J. Anal. Appl. Pyrolysis 79 (2007) 147–153, https://doi.org/10.1016/j.jaap.2006.12.005.
[29] M.R. Rover, L.E. Whitmer, R.G. Smith, R.C. Brown, The Effect of Pyrolysis Temperature on Recovery of Bio-oil As Distinctive Stage Fractions, (2016), https://doi.org/10.1016/j.jaap.2013.11.012.
[30] A.S. Pollard, M.R. Rover, R.C. Brown, Characterization of bio-oil recovered as stage fractions with unique chemical and physical properties, J. Anal. Appl. Pyrolysis 93 (2012) 129–138, https://doi.org/10.1016/j.jaap.2011.10.007.
[31] D. Mohan, C.U. Pittman, P.H. Steele, Pyrolysis of wood / biomass for bio-oil : a critical review, Energy Fuels 20 (2006) 848–889, https://doi.org/10.1021/ef0502397.
[32] A. Oasmaa, S. Czernik, Fuel oil quality of biomass pyrolysis oil - State of the art for the end users, Energy Fuels 13 (1999) 914–921, https://doi.org/10.1021/ef980272b.
[33] N. Priharto, F. Ronsse, W. Prins, I. Hita, P.J. Deuss, H.J. Heeres, Hydrotreatment of pyrolysis liquids derived from second-generation bioethanol production residues over NiMo and CoMo catalysts, Biomass Bioenergy 126 (2019) 84–93, https://doi.org/10.1016/j.biombioe.2019.05.005.
[34] X. Bai, K. Ho, R.C. Brown, E. Dalluge, C. Hutchinson, Y. Jin, D. Dalluge, Formation of phenolic oligomers during fast pyrolysis of lignin, Fuel 128 (2014) 170–179, https://doi.org/10.1016/j.fuel.2014.03.013.
[35] P.R. Patwardhan, R.C. Brown, B.H. Shanks, Understanding the Fast Pyrolysis of Lignin, 2230, (2011), pp. 1629–1636, https://doi.org/10.1002/cssc.201100133.
[36] P.R. Patwardhan, R.C. Brown, B.H. Shanks, Product Distribution From the Fast Pyrolysis of Hemicellulose, 2230, (2011), pp. 636–643, https://doi.org/10.1002/cssc.201000425.
[37] M. Ishikawa, M. Tamura, Y. Nakagawa, K. Tomishige, Demethoxylation of guaiacol and methoxybenzenes over carbon-supported Ru – Mn catalyst, Appl. Catal. B Environ. 182 (2016) 193–203, https://doi.org/10.1016/j.apcatb.2015.09.021.
[38] M.B. Figueirêdo, P.J. Deuss, R.H. Venderbosch, H.J. Heeres, Valorization of pyrolysis liquids: ozonation of the pyrolytic lignin fraction and model components, ACS Sustain. Chem. Eng. 7 (2019) 4755–4765, https://doi.org/10.1021/acssuschemeng.8b04856.
[39] G. Yildiz, T. Lathouwers, H.E. Toraman, K.M. Van Geem, G.B. Marin, F. Ronsse, R. Van Duren, S.R.A. Kersten, W. Prins, Catalytic fast pyrolysis of pine wood: effect of successive catalyst regeneration, Energy Fuels 28 (2014) 4560–4572, https://doi.org/10.1021/ef500636c.
[40] Z. Ma, E. Troussard, J.A. Van Bokhoven, Controlling the selectivity to chemicals from lignin via catalytic fast pyrolysis, Appl. Catal. A Gen. 423–424 (2012) 130–136, https://doi.org/10.1016/j.apcata.2012.02.027.
[41] T. Mochizuki, S. Chen, M. Toba, Y. Yoshimura, Pyrolyzer – GC / MS system-based analysis of the effects of zeolite catalysts on the fast pyrolysis of Jatropha husk, Appl. Catal. A Gen. 456 (2013) 174–181, https://doi.org/10.1016/j.apcata.2013.02.022.
[42] J. Piskorz, P. Majerski, D. Radlein, Pyrolysis of biomass - aerosol generation: properties, applications, and significance for process engineers, in biomass, a growth opportunity in Green energy and value-added products, 4th Biomass Conf. Am. (1999) 1153–1159.
[43] J.E. Peters, J.R. Carpenter, D.C. Dayton, Anisole and Guaiacol Hydrodeoxygenation Reaction Pathways Over Selected Catalysts, (2015), https://doi.org/10.1021/ef502551p.
[44] M. Coma, F. Ronsse, W. Soetaert, W. Verstraete, K. Rabaey, Products recovery from lignocellulose-based biomass for carbon-negative bio-based economy, 14th World Congr. Anaerob. Dig. Vina Del Mar, Chile, 2015.